Atmospheric Environment 204 (2019) 22–31

Contents lists available at ScienceDirect

Atmospheric Environment

journal homepage: www.elsevier.com/locate/atmosenv

Neural network predictions of pollutant emissions from open burning of crop residues: Application to air quality forecasts in southern China

Xu Feng[a], Tzung-May Fu[a,*], Hansen Cao[a], Heng Tian[a], Qi Fan[b], Xiaoyang Chen[b]

[a] Department of Atmospheric and Oceanic Science, School of Physics, Peking University, Beijing, China
[b] School of Atmospheric Sciences, Sun Yat-sen University, Guangzhou, China

ARTICLE INFO

Keywords:
Crop residue burning
Biomass burning
Back-propagation neural network
Fire emission forecast
$PM_{2.5}$

ABSTRACT

Open burning of crop residues is a strong seasonal source of air pollutants in many parts of China, but the large day-to-day variability of the associated emissions pose a great challenge for air quality forecasts. Here we developed back-propagation neural network (BPNN) ensembles to forecast the daily fire pixel counts in Southern China during the month of January. The BPNN ensembles were trained using daily assimilated surface meteorological data (including air temperature, relative humidity, pressure, and winds) and daily fire pixel observations from the Moderate Resolution Imaging Spectroradiometer (MODIS) for the month of January during the years 2003–2012. We showed that the BPNN ensembles successfully forecasted the day-to-day variability and the interannual variability of fire pixel counts over Southern China in January of the years 2013–2015, with correlation coefficients of 0.6–0.8 against the MODIS observations. We used the forecasted daily fire pixel counts in January 2014 and January 2015 to scale the climatological January biomass burning emissions from the Fire Inventory from NCAR (FINN) and applied the resulting forecasted daily biomass burning emissions to drive the WRF-Chem regional air quality model. The use of BPNN-ensemble-forecasted daily biomass burning pollutant emissions led to significant improvements in the daily forecasts of $PM_{2.5}$ concentrations in Southern China for January 2014, with the mean bias of the simulated surface $PM_{2.5}$ concentrations reduced from −9.1% to −1.2%. We repeated the sensitivity simulations for January 2015 and also found a modest improvement when using the forecasted daily biomass burning pollutant emissions (mean bias of the simulated surface $PM_{2.5}$ concentrations reduced from −5.8% to −2%). Our approach can be applied to other source regions of biomass burning emissions to improve the accuracy of daily air quality forecasts.

1. Introduction

Open, in-field burning of crop residues, a type of biomass burning, is a strong seasonal source of air pollutants in many parts of China (Ding et al., 2013; Nie et al., 2015; Wang et al., 2015; Wu et al., 2017; Chen et al., 2017). Agricultural operations in China currently produce 500 to 700 Tg of crop residues per year (Li et al., 2016), 75% of which are in the form of straws of rice, wheat, and corn (Chen et al., 2017). Although the open burning of these crop residues has been outlawed since the year 2000, it has been estimated that 6.6%–28% of the national total crop residues are still being burned in-field (Cao et al., 2008; Huang et al., 2012; Li et al., 2016). In Southern China, it was estimated that 26%–38% of the total crop residues were burned in-field between the years 2000 and 2014 (Jin et al., 2018). This is because Chinese farmers no longer use crop residues as primary fuel for residential heating and cooking, and alternative means of disposing large amounts of crop residues are costly and inconvenient (Qu et al., 2012; Zhao et al., 2017).

The occurrences of open crop residue burning in China are highly variable in space and time. Seasonally, the spatial distribution of these burning activities are tied to the harvest of local crops, e.g., the harvest of winter wheat over the North China Plain in June and the harvest of late rice over Southern China from December to the following February (Huang et al., 2012; Zha et al., 2013; Zhuang et al., 2018). In addition, the occurrences of these burning activities vary greatly from day to day and may have strong, implicit dependencies on local meteorology. For example, cold temperature and large precipitation during the growing season, particularly during the final crop-ripening stage, may delay the harvest and the subsequent open burning dates by up to 10 days (Wang et al., 2009). Moreover, crop residues do not burn in the field during rain, or farmers may choose not to ignite the residues when they are damp. Crop residue burning activities may also be affected by local socio-economical factors, such as the differences in crop types and

* Corresponding author. Department of Atmospheric and Oceanic Sciences, School of Physics, Peking University, Beijing, 100871, China.
E-mail address: tmfu@pku.edu.cn (T.-M. Fu).

https://doi.org/10.1016/j.atmosenv.2019.02.002
Received 6 November 2018; Received in revised form 25 January 2019; Accepted 3 February 2019
Available online 08 February 2019

harvesting techniques, the enforcement of anti-burning laws, and the infrastructure for recycling crop residues, etc (Qu et al., 2012).

The large day-to-day variability of the crop residue burning activities poses a great challenge for regional air quality forecasts. Many biomass burning emission inventories use surface reports or satellite observations of fire pixels, burned area, or fire radiative power to represent the spatiotemporal variability of fires (e.g., van der Werf et al., 2006, 2010; 2017; Larkin et al., 2009; Wiedinmyer et al., 2011; Huang et al., 2012; Li et al., 2016). In an air quality hindcast, these inventories can provide daily, km-scale-resolution estimates of pollutant emissions from biomass burning, including the open burning of crop residues and other types of biomasses. In an air quality forecast, however, there is currently no good way to predict the day-to-day variability of fire activities. Most air quality forecast models either ignored the biomass burning emissions (e.g., Wang et al., 2012) or, more commonly, used the monthly mean biomass burning emissions for all days in the same month, leading to gross inaccuracies in daily air quality forecasts. (e.g., Chen et al., 2009; Li et al., 2013b). Some air quality models "forecasted" biomass burning by assuming that the fire conditions observed in near-real-time will persist for a few days, either with or without modulation in fire intensities and/or fire counts by weather (e.g., Larkin et al., 2009; Kochanski et al., 2013; Peterson et al., 2013; Pavlovic et al., 2016; Di Giuseppe et al., 2017). This assumption is likely not applicable to fires that are small in scale, short in duration, and heavily manipulated by humans, such as the fires associated with crop residue burning.

A number of studies have developed process-based fire schemes for climate models and have included meteorological influences on the occurrence, strength, and spread of fires (e.g., Arora and Boer, 2005; Pechony and Shindell, 2009; Li et al., 2012, 2013a). For example, Li et al. (2012, 2013a) parameterized fire occurrences as a function of cloud-to-ground lightning flash rates, relative humidity, and soil wetness. In addition, they linked the spread of fires to the directions and speeds of surface winds and the degree of fire suppression by human. Li et al. (2013a) showed that their global fire parameterization reproduced the observed seasonal and interannual variability of global burned area between 1997 and 2004. However, whether these parameterizations developed for climate models were able to reproduce the observed day-to-day variability of small fires remained unknown.

We propose here the use of back-propagation artificial neural networks (BPNNs) (Rumelhart et al., 1986) to forecast the day-to-day variability of open crop residue burning activities. BPNNs learn from historical datasets - in our case the historical daily meteorological data and fire pixel counts - and find the empirical relationships between the variables. Several studies have used artificial neural networks to predict the seasonal and daily risk of forest wildfires (Vasconcelos et al., 2001; Li et al., 2009; Vasilakos et al., 2009; Stair et al., 2016). These studies showed that the risk of forest wildfires are generally positively correlated with temperature, while being negatively correlated with rainfall, relative humidity, and soil moisture, and non-linearly dependent on population density. To the best of our knowledge, the use of artificial neural networks to forecast the day-to-day variability of open crop residue burning activities have not yet been explored.

As a proof of concept, we developed BPNN ensembles to forecast the daily fire pixel counts and the associated biomass burning emissions in Southern China (domain D03 in Fig. 1a) for January from the years 2013–2015. We focused on the month of January, when the fire pixel counts in Southern China were largest in the year (Zhuang et al., 2018) and more than 90% of the local biomass burning emissions were associated the post-harvest burning of the straws from third-round late rice (Yan et al., 2006; He et al., 2011; Huang et al., 2012). We applied the forecasted biomass burning pollutant emissions in an air quality model and compared the simulated $PM_{2.5}$ concentrations to observations in January 2014 and January 2015, with the goal of assessing the effectiveness of the BPNNs in improving regional air quality forecasts.

2. Methodology

2.1. Fire pixel observations and surface meteorological data

We divided the Southern China domain into eight 3° longitude × 2° latitude boxes (Fig. 1) and trained BPNN ensembles independently for each box (Section 2.2) to account for the local socio-economical impacts on crop residue burning. We calculated the daily fire pixel counts and daily mean values of the surface meteorological variables within each of the eight boxes. Daily surface meteorological data during the month of January for the years 2003–2015 were taken from the National Centers for Environmental Prediction (Final) Operational Global Analyses dataset (NCEP FNL) (Kalnay et al., 1996), which had a spatial resolution of 1° × 1° and a temporal resolution of six hours. We verified that these reanalysis data were consistent with surface meteorological measurements over Southern China during January of 2003–2012.

We used the daily fire location data from the Global Monthly Fire Location Product (MCD14ML, Collection 5; Giglio, 2013) during the month of January for the years 2003–2015, observed by the MODIS instruments on board the Terra and Aqua satellites. Terra and Aqua are both polar-orbiting satellites, overpassing the Equator in the descending mode at 10:30 local time (LT) and 14:30 LT, respectively. The fire detection algorithm for the MCD14ML dataset was described in detail in Giglio (2013). Briefly, the algorithm classified each 1-km pixel within the MODIS swaths into one of the following six classes: fire, non-fire, cloud, water, unknown, or missing data. Over land, potential fire pixels were identified based on enhancements in the brightness temperatures in the mid-infrared channels (4 μm and 11 μm) relative to the non-fire background. False fire detections due to sun glint and desert surfaces were removed. Cloud pixels were identified by high reflectance in the visible channels and/or low brightness temperatures in the 12 μm channel. A detection confidence was calculated for each fire pixel based on five criteria (Giglio et al., 2003). We used only fire pixels with detection confidence exceeding 50%, which amounted to 84% of the fire pixels reported in the MCD14ML dataset for the month of January between 2003 and 2015. Theoretically, fire pixels may be "double-counted" if the area was sampled more than once by the MODIS swaths on a given day. However, this was not a major issue for our case, as only 1.3% of the pixels (205 fire pixels out of a total of 15759 fire pixels) were reported as fire more than once on any given day during the month of January between 2003 and 2015.

Cloud may obstruct the satellite detection of fire/non-fire conditions at the surface, although this did not seem to be a major issue for the domain and the time period of our study. For our domain in Southern China, the January mean fractions of MODIS-sampled pixels identified as clouds between 2003 and 2015 were relatively low (4.6%–24.9%, average 15%). The correlation between the daily fire pixel counts and the daily fractions of cloud-covered pixels over Southern China in January from the year 2003–2015 was also low ($R = -0.35$, 403 samples). We will return to the impacts of cloud on fire pixel detection in Section 3.

In this study, we chose to use the MCD14ML Collection 5 product so as to be consistent with the Fire INventory from NCAR (FINN; Wiedinmyer et al., 2011), which we scaled to forecast daily biomass burning emissions (described in Section 2.3 below). An updated Collection 6 fire product is also available from MODIS (Giglio, 2015). We compared the daily fire pixel counts from Collection 5 and Collection 6 over Southern China during the month of January for the years 2003–2015 (Fig. S1). We found that, although the daily fire pixel counts over Southern China in Collection 6 were systematically larger than those in Collection 5 by 73%, the correlation coefficient between the two products was 0.9. As such, the day-to-day variability of the two products were highly consistent with each other.

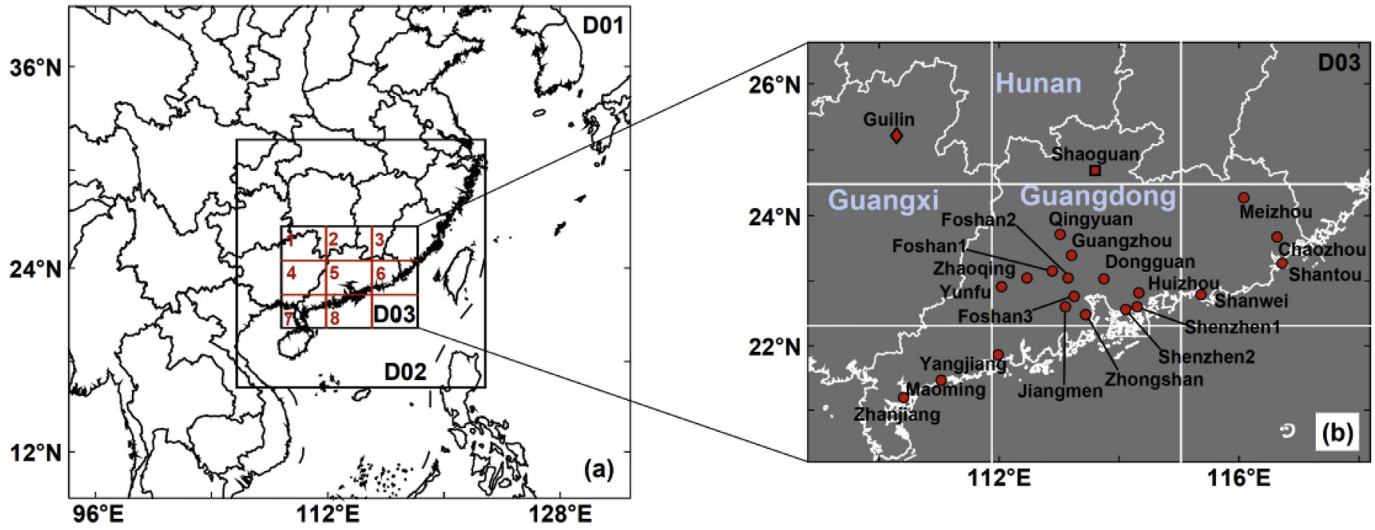

Fig. 1. (a) The three nested domains in our WRF-Chem simulations, with horizontal resolutions of 81 km, 27 km, and 9 km, respectively. The innermost domain (D03) covering Southern China was divided into eight boxes (red) for analyses; a BPNN ensemble was developed for each of these eight boxes. (b) The Southern China domain (D03) and the locations of the 22 surface $PM_{2.5}$ measurement sites (red symbols). The sites Guilin (red diamond) and Shaoguan (red square) are marked. (For interpretation of the references to colour in this figure legend, the reader is referred to the Web version of this article.)

2.2. BPNN ensembles of fire pixel counts

For each of the eight boxes over Southern China, we constructed a BPNN ensemble of 100 members to parameterize the relationships between fire pixel counts and surface meteorological variables. Each individual BPNN member was trained using daily data from the month of January during the years 2003–2012. The January data from the years 2013–2015 were reserved for validation (Section 3).

Fig. 2 shows our three-layer structure for each BPNN member, which consisted of an input layer, a hidden layer, and an output layer. Through trial and error, we found this structure to be the simplest one that served our need. The superscript s denoted the input/output data for a particular day. The input layer consisted of N_I neurons. I_i^s, the signal transmitted by the ith neuron in the input layer, was the value of the ith input surface meteorological variable linearly mapped to a range of [-1, 1]. The hidden layer consisted of N_H neurons, each conducting an intermediate calculation on the transmitted signals from the input layer. The signal transmitting out of the hth hidden neuron was

$$H_h^s = f\left(\sum_{i=1}^{N_I} I_i^s \cdot W_{i,h}^H + B_h^H\right) \tag{1a}$$

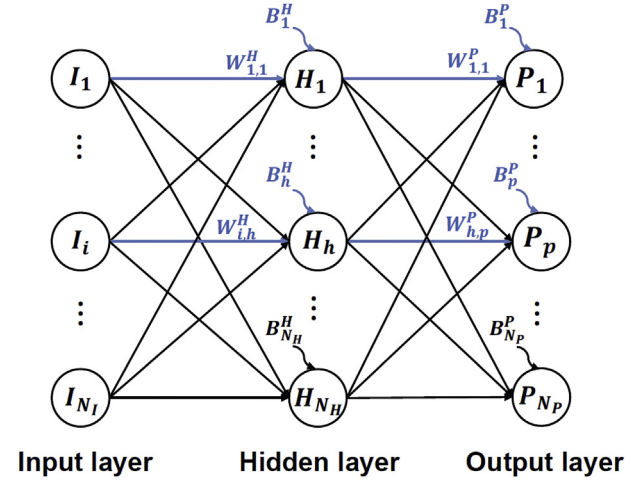

Fig. 2. The BPNN structure used in this study.

$$f(X) = \frac{e^X - e^{-X}}{e^X + e^{-X}} \tag{1b}$$

where $W_{i,h}^H$ was the weight applied to the I_i^s signal and B_h^H was a systematic bias applied by the hth neuron in the hidden layer. We selected the activation function, f, to be the continuous and non-linear tangent sigmoid function (Eq. (1b)). The output layer consisted of N_p neurons. The signal transmitted by the pth neuron in the output layer was

$$P_p^s = g\left(\sum_{h=1}^{N_H} H_h^s \cdot W_{h,p}^P + B_p^P\right) \tag{2a}$$

$$g(X) = X \tag{2b}$$

where $W_{h,p}^P$ was the weight applied to the transmitted signal from the hth neuron in the hidden layer by the pth neuron in the output layer, and B_p^P was a systematic bias assumed by the pth neuron in the output layer. In our case, there was only one output neuron ($N_P = 1$). We chose the activation function, g, to be the identity function, such that the transmitted value from the output layer was the predicted daily fire pixel counts for the box of interest.

By "training" a BPNN member, we sought to minimize a cost function, J, defined as

$$J = \frac{1}{S}\sum_{s=1}^{S} (P_{p=1}^s - Y_{p=1}^s)^2 \tag{3}$$

where $Y_{p=1}^s$ was the daily MODIS-observed fire pixel counts for the box of interest, and S was the length of the training data (31 days × 10 years). The coefficients in the BPNN were iteratively optimized using a Levenberg-Marquardt algorithm (Hagan and Menhaj, 1994) until one of two convergence criteria was achieved: (1) J was reduced to less than 1% of its initial value, or (2) further decreases in J could not be achieved using a Newtonian method after ten consecutive iterations (i.e., a local minimum of J was found). Each of the 100 member of a BPNN ensemble was trained with randomized initial guesses for the coefficients; this allowed the optimization algorithm to converge to more than one possible solution and achieve better generalization.

In order to select the meteorological variables to use as inputs to the BPNNs, we first picked out the daily surface meteorological variables from the NCEP FNL dataset that were significantly correlated with the daily fire pixel counts over Southern China. We then added these

Table 1
Sensitivity simulations of surface $PM_{2.5}$ concentrations over Southern China in January 2014.

Experiments	Daily biomass burning emissions	Mean concentration (unit: μg m^{-3}) and normalized mean biases (NMB) against the measurements[a]
FINN_2014	Daily biomass burning emissions taken from FINN for January 2014	72.1 (−7.9%)
NO_BB	No biomass burning emissions	65.0 (−17.0%)
FINN_MEAN	Climatological biomass burning emissions from FINN for the month of January during the years 2003 to 2012	71.1 (−9.1%)
BPNN_2014	Daily biomass burning emissions forecasted by scaling FINN climatology emissions with daily fire pixel counts forecasted by the BPNN ensembles for January 2014	77.3 (−1.2%)

[a] Calculated for January 4th to 31st, 2014.

meteorological variables one by one to the BPNN and performed training experiments. Through a series of BPNN training experiments, we selected five surface meteorological variables (air temperature, relative humidity, air pressure, *U*-wind, and *V*-wind) as inputs ($N_I = 5$) and two neurons in the hidden layer ($N_H = 2$), on the account that this combination of input variables and hidden layer structure predicted daily fire pixel counts that agreed best with the MODIS observations in January 2014 (Section 3).

2.3. Daily biomass burning emission forecasts

To forecast the daily fire pixel counts for January 2013 to 2015, we drove the BPNN ensemble with daily mean values of surface meteorological variables from the NCEP FNL reanalysis dataset, in order to focus our assessment on the predictive power of the BPNN ensembles. In an actual forecast, the BPNN ensembles may be driven by outputs from the NCEP Global Forecast System or other meteorological forecasts, but the accuracy of the forecasted fire pixel counts would be affected by the accuracy of the meteorological forecasts. For each box of interest, we took the daily ensemble average as our forecasted daily fire pixel counts.

In order to forecast the daily biomass burning emissions over Southern China, we used the forecasted daily fire pixel counts to scale the climatological biomass burning emissions from FINN (version 1.5; Wiedinmyer et al., 2011). FINN was developed at 1-km resolution using daily fire pixel locations from the MCD14ML dataset (Collection 5; Giglio et al., 2006), as well as the Land Cover Type product (Friedl et al., 2010) and the Vegetation Continuous Fields product (Hansen et al., 2003; 2005; Carroll et al., 2011) from MODIS. Emission factors used in FINN were taken from published literature (Andreae and Merlet, 2001; McMeeking, 2008; Akagi et al., 2011).

For an emitted trace species *m*, we forecasted the daily biomass burning emission ($E_{m,n,d}$ (*x*,*y*)) at location (*x*,*y*) in the *n*th box in Southern China on the *d*th day in January as:

$$E_{m,\,n,d}(x,\,y) = \overline{FINN\_E}_{m,\,n}(x,\,y)\cdot k_{n,d} \tag{4a}$$

$$k_{n,d} = \frac{FC_{n,d}}{\overline{FC}_n} \tag{4b}$$

where $\overline{FINN\_E}_{m,\,n}(x,\,y)$ was the climatological biomass burning emission for species *m* at location (*x*,*y*) in the *n*th box from FINN, calculated by averaging over all days in January for the years 2003–2012 (the time period used for training the BPNN ensembles). The daily fire activity scale factor, $k_{n,d}$, was defined as the ratio between the BPNN-ensemble-forecasted fire pixel counts on the *d*th day in the *n*th box ($FC_{n,d}$) and the climatological fire pixel counts in the *n*th box for all days in January 2003 to 2012 ($\overline{FC}_n$).

2.4. WRF-Chem sensitivity experiments and surface $PM_{2.5}$ observations

We used the Weather Research and Forecasting model coupled with Chemistry (WRF-Chem, version 3.6.1, Grell et al., 2005) to simulate surface $PM_{2.5}$ concentrations over Southern China in January 2014 and January 2015. Fig. 1a shows the three nested model domains with spatial resolutions of 81 km (50 × 44 grids), 27 km (66 × 66 grids), and 9 km (108 × 81 grids), respectively. The innermost domain covered Southern China (Fig. 1b). Meteorological boundary conditions used to drive WRF-Chem were from the NCEP FNL dataset and updated every six hours. We used the monthly mean tracer concentrations simulated by the MOZART-4 global model (Emmons et al., 2010) as chemical initial/boundary conditions. Aerosol species in our model included primary elemental carbon aerosols, primary organic aerosols, dust, sea salt, other primary $PM_{2.5}$, secondary inorganic aerosols, and secondary organic aerosols (SOA). Emission inventories for anthropogenic and biogenic sources were as described in the supplementary information and interpolated to the model grids. Aerosol microphysics and secondary aerosol formation was simulated with the MOSAIC module using four size bins (Zaveri et al., 2008). SOA formation was simulated using the volatility basis set framework (Shrivastava et al., 2011). The simulations were conducted from January 1st to 31st, 2014; the first three days initialized the model.

We conducted four sensitivity simulations each for January 2014 and January 2015, respectively, using different biomass burning emissions. As summarized in Table 1 for January 2014, we first conducted a simulation (FINN_2014) where the daily biomass burning emissions over Southern China were as given by FINN for January 2014. This simulation represented a best-case scenario, where the day-to-day variability of biomass burning emissions was described by the daily actual fire observations from satellites. Secondly, we conducted a simulation (NO_BB) where the biomass burning emissions over Southern China were turned off. A third simulation (FINN_MEAN) was conducted where the daily biomass burning emissions over Southern China were set to the climatological January mean biomass burning emissions from FINN for the years 2003–2012. This simulation represented the approach most commonly taken by current air quality models in the forecast mode. Finally, a fourth simulation (BPNN_2014) was driven by our BPNN-ensemble forecasted daily biomass burning emissions. A similar set of sensitivity simulations was conducted for January 2015 (Table S2).

We compared our simulated $PM_{2.5}$ concentrations to hourly measurements during January 2014 and January 2015 at surface sites managed by the China National Environmental Monitoring Centre (www.cnemc.cn). We removed obvious erroneous measurements and excluded sites with less than 90% valid hourly measurements (supplementary information). Some model grids contained more than one surface site. In such cases, we selected the site with the most complete valid hourly measurements during January 2014 and 2015. In the end, measurements from 22 surface sites were used for comparison with our simulations (Fig. 1b and Table S1).

3. BPNN ensemble forecasts of daily fire pixel counts and biomass burning emissions

Fig. 3 shows the daily fire pixel counts forecasted by our BPNN ensembles and compares them against the daily fire pixel counts observed by MODIS for each of the eight boxes of interests in January

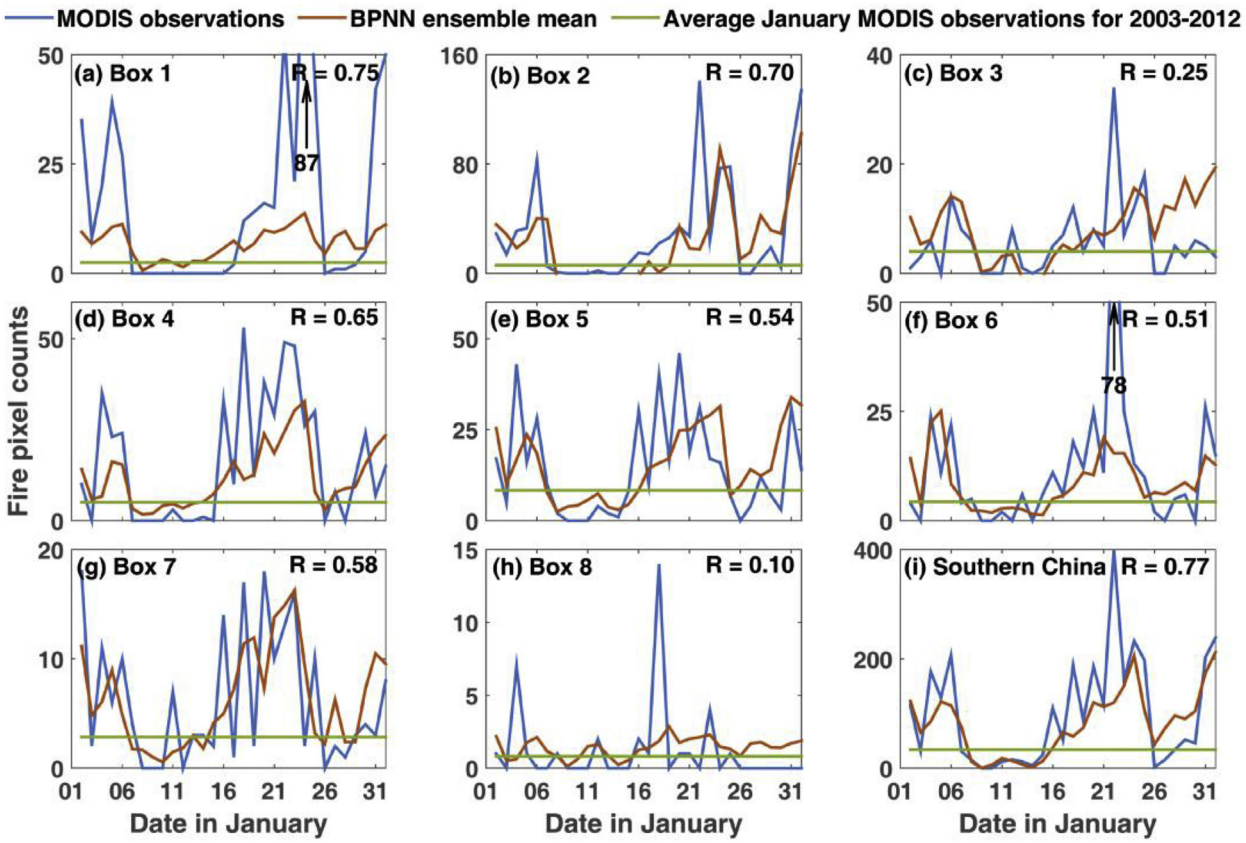

Fig. 3. Comparison of the daily fire pixel counts as observed by MODIS (blue lines) and as forecasted by the BPNN ensembles (red lines) for January 2014: ((a) to (h)) for each of the eight boxes of interest and (i) for the Southern China domain. Also shown are the climatological MODIS fire pixel count for January during the years 2003–2012 (green lines).

2014. Also shown in Fig. 3 are the climatological January mean fire pixel counts observed by MODIS during the years 2003–2012. The MODIS-observed fire pixel counts showed two periods of high values: one during January 1st to 7th, 2014 and one during January 16th to 25th, 2014. The lowest and highest MODIS-observed daily fire pixel counts within a given box were 0 and 141, respectively. This large day-to-day variation in fire occurrences could not be represented by the climatological January fire pixel counts. In contrast, our forecasted daily fire pixel counts reproduced the day-to-day variation of the MODIS observations, with correlation coefficients (R) exceeding 0.50 for six of the eight boxes and R = 0.77 for the Southern China domain.

The BPNN ensembles were also able to capture the interannual variation of fire activities over Southern China. Fig. 4 compares the daily fire pixel counts over Southern China forecasted by our BPNN ensembles for January 2013, 2014, and 2015, against those observed by MODIS. The correlation coefficients between the forecasted and observed daily fire pixel counts were 0.60, 0.77, and 0.80 for January 2013, 2014, and 2015, respectively. The MODIS-observed mean fire pixel count in January 2013 was 13, which was much smaller than those in January 2014 (100) and January 2015 (37). We found that this difference was not entirely due to obstruction by clouds in January 2013, as the fraction of MODIS-sampled pixels covered by clouds were both 13% in January 2013 and 2015. Moreover, the fraction of MODIS-sampled pixels covered by clouds in January 2009 was also 13%, but the fire pixel count in January 2009 was 94, much higher than the fire pixel counts for either January 2013 or January 2015. Instead, the lower fire pixel counts in January 2013 was at least partially due to a cold growing season and delayed harvest. According to surface meteorological records and the NCEP FNL data, Southern China suffered episodes of freezing rain and snow in early January 2013, and the regional mean temperature was 1.9 °C colder than the climatology. As a result, the harvest of late rice in 2013 were 2.7% lower than that in 2009 and 7.0% lower than that in 2015, according to the Guangdong Statistical Yearbook of Agriculture (Xing et al., 2014). Our BPNNs partially captured this interannual difference: the forecasted mean fire

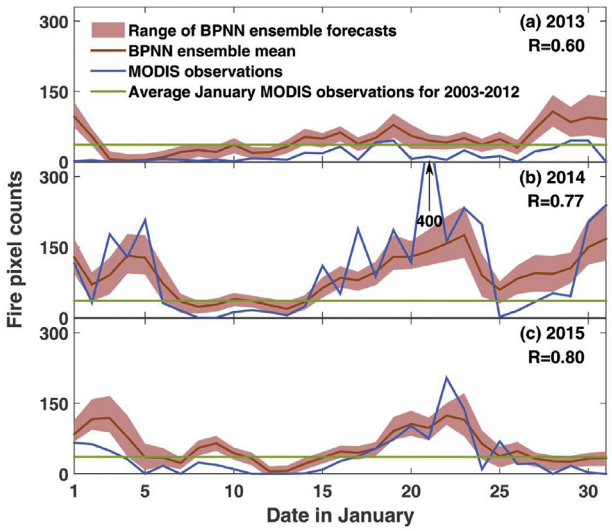

Fig. 4. Comparison of the daily fire pixel counts over the Southern China domain as observed by MODIS (blue lines) and as forecasted by the BPNN ensembles (red lines and red shading areas indicate the means and the ranges of the BPNN ensemble forecast, respectively) for January (a) 2013, (b) 2014, and (c) 2015. Also shown are the MODIS-observed fire pixel count climatology for January during the years 2003–2012 (green lines).

Table 2
Comparison of the performances of BPNN ensembles in forecasting fire pixel counts over Southern China in January during the years 2013–2015.

		MODIS observed daily fire pixel counts	Full BPNN ensemble[a]	Sensitivity BPNN ensemble experiments[b]					
				RH_clim	T_clim	P_clim	U_clim	V_clim	All_clim except RH[c]
2013	Monthly mean	13	46						
	RMSE [R][d]		40.0 [0.6]	113 [0.39]	116 [0.04]	114 [0.11]	115 [0.16]	115 [0.11]	122 [-0.28]
2014	Monthly mean	100	89						
	RMSE [R]		68.6 [0.77]	108 [0.29]	73.8 [0.72]	71.7 [0.75]	71.3 [0.76]	72.8 [0.75]	84.6 [0.73]
2015	Monthly mean	37	56						
	RMSE [R]		33.3 [0.80]	109 [0.43]	98 [0.47]	95.5 [0.47]	96.6 [0.47]	97.2 [0.45]	108 [0.33]

[a] The full BPNN ensembles were trained using the daily values of all five surface meteorological variables (T, P, RH, U, and V).
[b] The sensitivity BPNN ensembles were trained by setting the daily values of select meteorological variables to their January climatology values.
[c] Only the daily values of RH were used to train the BPNN ensembles. The values of all other meteorological variables were set to their climatological values.
[d] Root mean square error (RMSE) and correlation coefficient (R, shown in square brackets) against the MODIS observations.

pixel counts over Southern China for January 2013, 2014, and 2015 were 46, 89, and 56, respectively.

In order to better understand the implicit relationships between the daily surface meteorological conditions and fire activities, we conducted sensitivity experiments where we replaced the daily values of each of the five surface meteorological variables with their January climatological values (averaged over 2003 to 2012) and re-trained the BPNN ensembles. Table 2 compares the performances of the BPNN ensembles from these sensitivity experiments. The performance of the BPNN ensembles reduced dramatically when the day-to-day variability of relative humidity was removed from the training dataset: the correlation coefficients between the forecasted and MODIS-observed daily fire pixel counts for January 2013, 2014, and 2015 decreased to 0.39, 0.29, and 0.43, respectively. This declination in performance was easy to understand, as surface relative humidity has strong association with precipitation and the dampness of crop residues and should be a dominant predictor for fire activities. Surface relative humidity and surface temperature often show a strong negative correlation. As a result, the performance of the BPNN ensembles both decreased in January 2013 and January 2015 when the daily variability of surface air temperature was removed from the training dataset.

We found that the daily variability of surface pressure and horizontal winds were also implicitly linked to the daily variability of fire activities, although the mechanisms for such linkages remained unclear. The correlations between the forecasted and MODIS-observed fire pixel counts decreased significantly when the daily variability of surface pressure, *U*-wind, or *V*-wind was removed, particularly for January 2013. In addition, the BPNN ensembles were unable to forecast the day-to-day variability of fire pixel counts when driven only by the variability of relative humidity. We suspected that the variability of surface pressure and horizontal winds may (1) partially represent the impacts of short-term climate anomalies during the growing season, or (2) help manifest the nonlinear dependencies between relative humidity, temperature, and fire activities in the BPNNs.

Fig. 5 shows the spatial distributions of primary elemental carbon emissions from biomass burning as forecasted by our BPNN ensembles on three individual days in January 2014, as well as those given by FINN and by the January climatology of FINN. Our forecasted daily biomass burning emissions reflected not only the day-to-day variability of emission strengths, but also the relative changes in spatial patterns. For example, on January 3rd, 2014, FINN (based on MODIS-observed fire pixels) indicated more biomass burning emissions over northern Guangdong but less in western Guangdong and eastern Guangxi. In contrast, on January 23rd, 2014, FINN indicated relatively more biomass burning emissions over western Guangdong and eastern Guangxi. These relative changes in pollutant emissions were reproduced by our BPNN ensemble forecasts. On January 8th, 2014, FINN indicated very little biomass burning emissions across Southern China, which was also reproduced by our BPNN ensemble forecasts. These relative changes in the temporal and spatial distributions of pollutant emissions have large impacts on the local air quality and were not reflected in the climatological January emission from FINN.

4. Application to daily $PM_{2.5}$ forecasts over southern China in January 2014 and January 2015

Finally, we conducted sensitivity simulations using different biomass burning emissions, with the goal of evaluating the performance of our BPNN-ensemble predicted biomass burning emissions in air quality forecasts. Fig. 6a shows relative difference between the mean surface $PM_{2.5}$ concentrations from the "FINN_2014" case and those from the "NO_BB" case, which represents the fraction of simulated surface $PM_{2.5}$ concentrations resulting from biomass burning emissions during January 2014. Biomass burning emissions accounted for more than 40% of the simulated mean surface $PM_{2.5}$ concentrations over northern Guangdong, eastern Guangxi, and southern Hunan, indicates that the locations of croplands and thus crop residue burning activities in these areas.

Fig. 6b, c, and 6d compare the spatial distribution of the $PM_{2.5}$ concentrations simulated by the three sensitivity experiments against the surface $PM_{2.5}$ measurements over Southern China for January 4th to 31st, 2014. In all three experiments, the model simulated $PM_{2.5}$ concentrations exceeding 100 $\mu g\, m^{-3}$ in the central Pearl River Delta area, mainly reflecting the strong anthropogenic emissions from the megacities in the vicinity. In both the FINN_2014 and the BPNN_2014 experiments, high concentrations of $PM_{2.5}$ were also simulated over northern Guangdong, eastern Guangxi, and southern Hunan, reflecting the impacts of biomass burning. In particular, both simulations were able to reproduce the enhancements in $PM_{2.5}$ concentrations near Shaoguan (northern Guangdong) and Guilin (eastern Guangxi). In contrast, in the FINN_MEAN experiment, the $PM_{2.5}$ concentration enhancements were much weaker in the main biomass burning areas, and the high $PM_{2.5}$ concentrations measured at Shaoguan and Guilin were not reproduced.

Fig. 7 further compares the observed and simulated $PM_{2.5}$ concentrations at the two surface sites most impacted by biomass burning: Shaoguan and Guilin. At both sites, the omission of biomass burning emissions (NO_BB experiment) led to severe low biases in the simulated $PM_{2.5}$ concentrations relative to the measurements, particularly during two main burning periods: January 4th to 8th and January 25th to 29th, 2014. At Shaoguan, with the exception of a few days between January 19th to 21st, 2014, both the FINN_2014 and the BPNN_2014 experiments were able to simulate the observed $PM_{2.5}$ concentrations better than the FINN_MEAN experiments. At Guilin, both the FINN_2014 and the BPNN_2014 experiments out-performed the FINN_MEAN experiment throughout January 2014.

Table 1 compares the average simulated $PM_{2.5}$ concentrations sampled at the 22 surface sites from the sensitivity experiments, as well

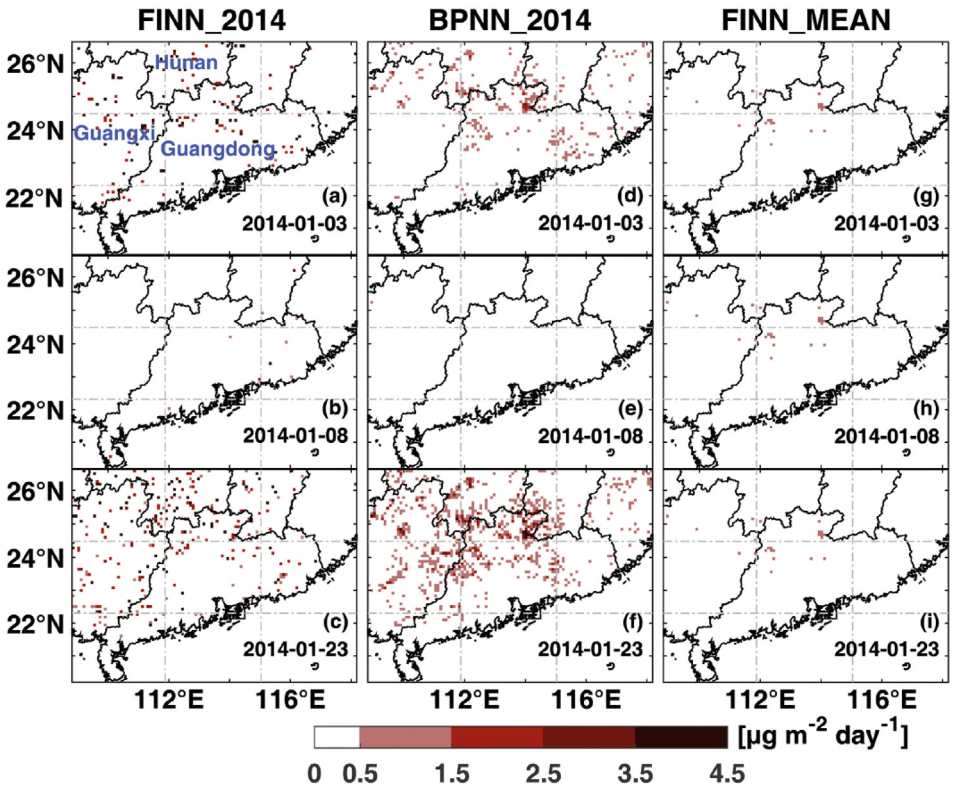

Fig. 5. The spatial distribution of the emission rates of primary elemental carbon from biomass burning (unit: μg m^{-2} day^{-1}) on January 3rd, 8th and 23rd, 2014 from (a), (b), (c): FINN; (d), (e), (f): the BPNN ensemble forecasts; and (g), (h), (i): the climatological FINN for January during the years 2003–2012. The provinces of Guangdong, Guangxi and Hunan are labeled in (a).

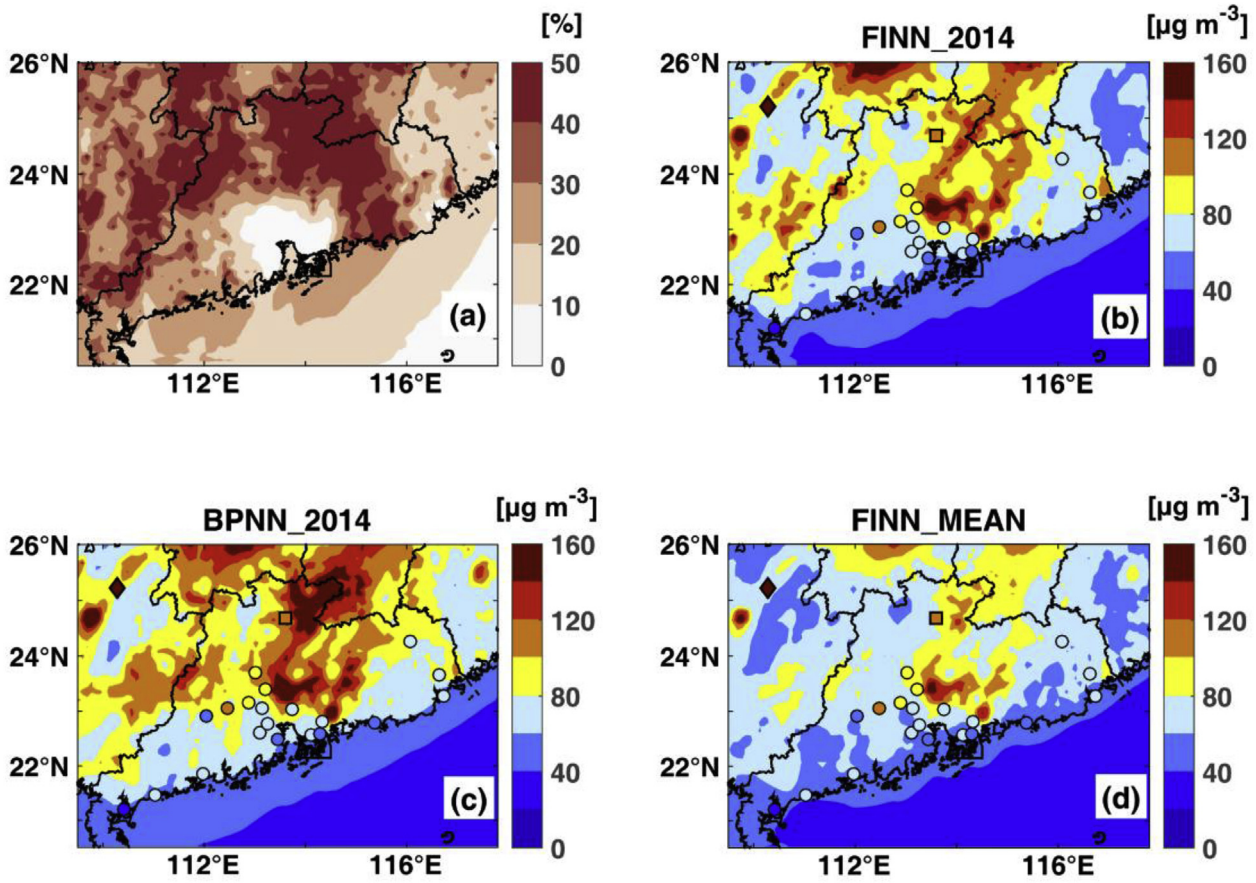

Fig. 6. (a) The fraction of surface $PM_{2.5}$ concentrations contributed by biomass burning emissions during Jan 4th to 31st, 2014. (b)–(d) Comparison of simulated (filled contours) and observed (filled symbols) $PM_{2.5}$ concentrations during Jan 4th to 31st, 2014 from (b) the FINN_2014 simulation, (c) the BPNN_2014 simulation, and (d) the FINN_MEAN simulation. The sites Guilin (filled diamond) and Shaoguan (filled square) are marked.

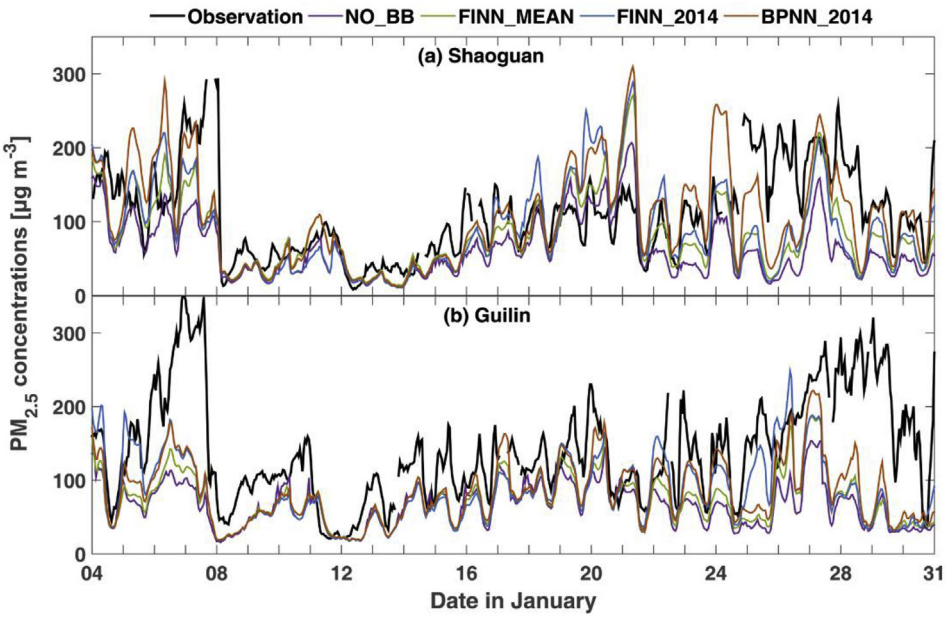

Fig. 7. Observed (black) and simulated hourly $PM_{2.5}$ mass concentrations at (a) Shaoguan and (b) Guilin during Jan 4th to 31th, 2014. The simulated concentrations from the four sensitivity experiments are shown: FINN_2014 (blue), BPNN_2014 (red), FINN_MEAN (green), and NO_BB (purple).

as the corresponding normalized mean biases (NMB) relative to the measurements during January 2014. The average $PM_{2.5}$ concentration measured at the 22 surface sites during January 4th to 31st, 2014 was 78.2 $\mu g\, m^{-3}$. The simulated $PM_{2.5}$ concentrations (sampled at the surface sites) in the FINN_2014 experiment averaged 72.1 $\mu g\, m^{-3}$, which was 7.9% lower than the measurements. As mentioned before, the FINN_2014 experiment represented the best-case scenario in a hindcast. However in reality, the most common approach taken by air quality forecasts was represented by the FINN_MEAN experiment, where the simulated $PM_{2.5}$ concentrations averaged 71.1 $\mu g\, m^{-3}$, 9.1% lower than the measurements. In contrast, when WRF-Chem was driven by our forecasted daily biomass burning emissions (BPNN_2014 experiment), the average simulated $PM_{2.5}$ concentration sampled at the surface increased to 77.3 $\mu g\, m^{-3}$, only 1.2% lower than the measurements. A similar set of sensitivity simulation were conducted for January 2015 (Table S2). We also found a modest improvement in the forecasted daily surface $PM_{2.5}$ concentrations when using the forecasted daily biomass burning emissions (BPNN_2015 experiment, NMB = −2.0%), compared to the experiment using the climatological biomass burning emissions (FINN_MEAN experiment, NMB = −5.8%). We thus concluded, from the analyses of Figs. 6 and 7, Table 1 and Table S2, that the use of our BPNN-ensemble daily biomass burning emission forecasts greatly improved the overall accuracy of the surface $PM_{2.5}$ concentration forecasts over Southern China in January, to the extent comparable to having explicit satellite-based fire observations to constrain the daily biomass burning emissions in a hindcast (i.e., FINN_2014 and FINN_2015 experiments).

5. Conclusions

We developed BPNN ensembles to forecast daily fire pixel counts over Southern China in January, with the goal of forecasting the day-to-day variability of emissions from the burning of biomasses (mainly crop residues), as well as improving the accuracy of $PM_{2.5}$ forecasts in this region. We used a decade's worth (2003–2012) of MODIS-observed daily fire pixel counts and assimilated daily surface meteorological data to train the BPNN ensembles. The resulting BPNN ensembles were able to forecast the day-to-day variability of the fire pixel counts over Southern China in January, with correlation coefficients against daily MODIS observations of 0.6–0.8 for the years 2013–2015. In addition, the BPNN ensembles were able to capture the interannual variability of fire pixel counts over Southern China, which likely reflected the impacts of interannual climate variability on the local crop harvest.

We used the forecasted daily fire pixel counts to scale the climatological January biomass burning emissions from FINN and applied the resulting forecasted daily biomass burning emissions to drive the WRF-Chem model. We found that the use of this daily biomass burning emission forecast led to significant improvements in the accuracy of the daily $PM_{2.5}$ forecasts in Southern China for January 2014, reducing the mean bias against surface $PM_{2.5}$ measurements from −9.1% to −1.2%. Similar improvements in the daily $PM_{2.5}$ forecasts were also found for January 2015, with the mean bias against surface measurements reduced from −5.8% to −2.0%. We thus concluded that the BPNN ensemble approach show significant skills in forecasting biomass burning emissions over Southern China, to the extent comparable to having explicit satellite-based fire observations.

6. Discussions

Our use of BPNNs to forecast the spatial and temporal variability of biomass burning emissions can be applied to other source regions. In theory, the BPNN ensemble may even potentially out-perform the satellite-based fire observations in representing fire activities. This is because satellite instruments cannot detect surface fires in pixels obscured by clouds. In contrast, given a sufficiently large training dataset, the BPNN ensembles can potentially learn to forecast fires based on the surface meteorological conditions, even at pixels obscured by clouds. This represents a potential advantage of the BPNN approach over the satellite observations but of course needs to be thoroughly validated with detailed surface fire observations. Other emerging satellite-based fire products, such as hourly surface hot spots from the Chinese FY-4A or the Japanese Himawari-8 geostationary satellites, may be explored to forecast surface fire activities at even higher temporal resolution. The use of BPNN or other machine learning techniques in forecasting pollutant emissions and air quality shows promise and warrants further investigation.

Declaration of interest statement

The authors declare that they have no competing interests, financial

or otherwise.

Acknowledgement

This work was supported by the Ministry of Science and Technology National Key R&D Program of China (2017YFC0209802) and the National Natural Sciences Foundation of China (41461164007).

Appendix A. Supplementary data

Supplementary data to this article can be found online at https://doi.org/10.1016/j.atmosenv.2019.02.002.

References

Akagi, S.K., Yokelson, R.J., Wiedinmyer, C., Alvarado, M.J., Reid, J.S., Karl, T., Crounse, J.D., Wennberg, P.O., 2011. Emission factors for open and domestic biomass burning for use in atmospheric models. Atmos. Chem. Phys. 11, 4039–4072. https://doi.org/10.5194/acp-11-4039-2011.

Andreae, M.O., Merlet, P., 2001. Emission of trace gases and aerosols from biomass burning. Glob. Biogeochem. Cycles 15, 955–966. https://doi.org/10.1029/2000gb001382.

Arora, V.K., Boer, G.J., 2005. Fire as an interactive component of dynamic vegetation models. J. Geophys. Res. Biogeo. 110, G02008. https://doi.org/10.1029/2005JG000042.

Cao, G.L., Zhang, X.Y., Wang, Y.Q., Zheng, F.C., 2008. Estimation of emissions from field burning of crop straw in China. Chin. Sci. Bull. 53, 784–790. https://doi.org/10.1007/s11434-008-0145-4.

Carroll, M., Townshend, J., Hansen, M., DiMiceli, C., Sohlberg, R., Wurster, K., 2011. MODIS Vegetative Cover Conversion and Vegetation Continuous Fields. In: Ramachandran, B., Justice, C.O., Abrams, M.J. (Eds.), Land Remote Sensing and Global Environmental Change: NASA's Earth Observing System and the Science of ASTER and MODIS. vol. 11. Springer, New York, NY, pp. 725–745. https://doi.org/10.1007/978-1-4419-6749-7.

Chen, J.M., Li, C.L., Ristovski, Z., Milic, A., Gu, Y.T., Islam, M.S., Wang, S.X., Hao, J.M., Zhang, H.F., He, C.R., Guo, H., Fu, H.B., Miljevic, B., Morawska, L., Thai, P., Fat, L.A.M.Y., Pereira, G., Ding, A.J., Huang, X., Dumka, U.C., 2017. A review of biomass burning: Emissions and impacts on air quality, health and climate in *China*. Sci. Total Environ. 579, 1000–1034. https://doi.org/10.1016/j.scitotenv.2016.11.025.

Chen, Y., Li, Q., Randerson, J.T., Lyons, E.A., Kahn, R.A., Nelson, D.L., Diner, D.J., 2009. The sensitivity of CO and aerosol transport to the temporal and vertical distribution of North American boreal fire emissions. Atmos. Chem. Phys. 9, 6559–6580. https://doi.org/10.5194/acp-9-6559-2009.

Di Giuseppe, F., Remy, S., Pappenberger, F., Wetterhall, F., 2017. Improving Forecasts of Biomass Burning Emissions with the Fire Weather Index. J. Appl. Meteorol. Clim. 56, 2789–2799. https://doi.org/10.1175/JAMC-D-16-0405.1.

Ding, A.J., Fu, C.B., Yang, X.Q., Sun, J.N., Petaja, T., Kerminen, V.M., Wang, T., Xie, Y., Herrmann, E., Zheng, L.F., Nie, W., Liu, Q., Wei, X.L., Kulmala, M., 2013. Intense atmospheric pollution modifies weather: a case of mixed biomass burning with fossil fuel combustion pollution in eastern China. Atmos. Chem. Phys. 13, 10545–10554. https://doi.org/10.5194/acp-13-10545-2013.

Emmons, L.K., Walters, S., Hess, P.G., Lamarque, J.F., Pfister, G.G., Fillmore, D., Granier, C., Guenther, A., Kinnison, D., Laepple, T., Orlando, J., Tie, X., Tyndall, G., Wiedinmyer, C., Baughcum, S.L., Kloster, S., 2010. Description and evaluation of the Model for Ozone and Related chemical Tracers, version 4 (MOZART-4). Geosci. Model Dev. (GMD) 3, 43–67. https://doi.org/10.5194/gmd-3-43-2010.

Friedl, M.A., Sulla-Menashe, D., Tan, B., Schneider, A., Ramankutty, N., Sibley, A., Huang, X.M., 2010. MODIS Collection 5 global land cover: Algorithm refinements and characterization of new datasets. Remote Sens. Environ. 114, 168–182. https://doi.org/10.1016/j.rse.2009.08.016.

Giglio, L., 2013. MODIS Collection 5 Active Fire Product User's Guide Version 2.5. Department of Geography, University of Maryland.

Giglio, L., 2015. MODIS Collection 6 Active Fire Product User's Guide Revision A. Department of Geography, University of Maryland.

Giglio, L., Csiszar, I., Justice, C.O., 2006. Global distribution and seasonality of active fires as observed with the Terra and Aqua Moderate Resolution Imaging Spectroradiometer (MODIS) sensors. J. Geophys. Res. Biogeo. 111, G02016. https://doi.org/10.1029/2005JG000142.

Giglio, L., Descloitres, J., Justice, C.O., Kaufman, Y.J., 2003. An enhanced contextual fire detection algorithm for MODIS. Remote Sens. Environ. 87, 273–282. https://doi.org/10.1016/S0034-4257(03)00184-6.

Grell, G.A., Peckham, S.E., Schmitz, R., McKeen, S.A., Frost, G., Skamarock, W.C., Eder, B., 2005. Fully coupled "online" chemistry within the WRF model. Atmos. Environ. 39, 6957–6975. https://doi.org/10.1016/j.atmosenv.2005.04.027.

Hagan, M.T., Menhaj, M.B., 1994. Training Feedforward Networks with the Marquardt Algorithm. Ieee. T. Neural Networ. 5, 989–993. https://doi.org/10.1109/72.329697.

Hansen, M.C., DeFries, R.S., Townshend, J.R.G., Carroll, M., Dimiceli, C., Sohlberg, R.A., 2003. Global percent tree cover at a spatial resolution of 500 meters: First results of the MODIS vegetation continuous fields algorithm. Earth Interact. 7, 1–15 https://doi.org/10.1175/1087-3562(2003)007 < 0001:GPTCAA > 2.0.CO;2.

Hansen, M.C., Townshend, J.R.G., Defries, R.S., Carroll, M., 2005. Estimation of tree cover using MODIS data at global, continental and regional/local scales. Int. J. Remote Sens. 26, 4359–4380. https://doi.org/10.1080/01431160500113435.

He, M., Zheng, J.Y., Yin, S.S., Zhang, Y.Y., 2011. Trends, temporal and spatial characteristics, and uncertainties in biomass burning emissions in the Pearl River Delta, China. Atmos. Environ. 45, 4051–4059. https://doi.org/10.1016/j.atmosenv.2011.04.016.

Huang, X., Li, M.M., Li, J.F., Song, Y., 2012. A high-resolution emission inventory of crop burning in fields in China based on MODIS Thermal Anomalies/Fire products. Atmos. Environ. 50, 9–15. https://doi.org/10.1016/j.atmosenv.2012.01.017.

Jin, Q.F., Ma, X.Q., Wang, G.Y., Yang, X.J., Guo, F.T., 2018. Dynamics of major air pollutants from crop residue burning in mainland China, 2000-2014. J. Environ. Sci-China. 70, 190–205. https://doi.org/10.1016/j.jes.2017.11.024.

Kalnay, E., Kanamitsu, M., Kistler, R., Collins, W., Deaven, D., Gandin, L., Iredell, M., Saha, S., White, G., Woollen, J., Zhu, Y., Chelliah, M., Ebisuzaki, W., Higgins, W., Janowiak, J., Mo, K.C., Ropelewski, C., Wang, J., Leetmaa, A., Reynolds, R., Jenne, R., Joseph, D., 1996. The NCEP/NCAR 40-year reanalysis project. Bull. Am. Meteorol. Soc. 77, 437–471 https://doi.org/10.1175/1520-0477(1996)077 < 0437:TNYRP > 2.0.CO;2.

Kochanski, A.K., Jenkins, M.A., Mandel, J., Beezley, J.D., Clements, C.B., Krueger, S., 2013. Evaluation of WRF-SFIRE performance with field observations from the FireFlux experiment. Geosci. Model Dev. (GMD) 6, 1109–1126. https://doi.org/10.5194/gmd-6-1109-2013.

Larkin, N.K., O'Neill, S.M., Solomon, R., Raffuse, S., Strand, T., Sullivan, D.C., Krull, C., Rorig, M., Peterson, J.L., Ferguson, S.A., 2009. The BlueSky smoke modeling framework. Int. J. Wildland Fire 18, 906–920. https://doi.org/10.1071/wf07086.

Li, F., Levis, S., Ward, D.S., 2013a. Quantifying the role of fire in the Earth system - Part 1: Improved global fire modeling in the Community Earth System Model (CESM1). Biogeosciences 10, 2293–2314. https://doi.org/10.5194/bg-10-2293-2013.

Li, F., Zeng, X.D., Levis, S., 2012. A process-based fire parameterization of intermediate complexity in a Dynamic Global Vegetation Model. Biogeosciences 9, 2761–2780. https://doi.org/10.5194/bg-9-2761-2012.

Li, J., Li, Y.Q., Bo, Y., Xie, S.D., 2016. High-resolution historical emission inventories of crop residue burning in fields in China for the period 1990-2013. Atmos. Environ. 138, 152–161. https://doi.org/10.1016/j.atmosenv.2016.05.002.

Li, L.M., Song, W.G., Ma, J., Satoh, K., 2009. Artificial neural network approach for modeling the impact of population density and weather parameters on forest fire risk. Int. J. Wildland Fire 18, 640–647. https://doi.org/10.1071/WF07136.

Li, N., Fu, T.M., Cao, J.J., Lee, S.C., Huang, X.F., He, L.Y., Ho, K.F., Fu, J.S., Lam, Y.F., 2013b. Sources of secondary organic aerosols in the Pearl River Delta region in fall: Contributions from the aqueous reactive uptake of dicarbonyls. Atmos. Environ. 76, 200–207. https://doi.org/10.1016/j.atmosenv.2012.12.005.

McMeeking, G.R., 2008. The Optical, Chemical, and Physical Properties of Aerosols and Gases Emitted by the Laboratory Combustion of Wildland Fuels. PhD Dissertation. Colorado State University.

Nie, W., Ding, A.J., Xie, Y.N., Xu, Z., Mao, H., Kerminen, V.M., Zheng, L.F., Qi, X.M., Huang, X., Yang, X.Q., Sun, J.N., Herrmann, E., Petaja, T., Kulmala, M., Fu, C.B., 2015. Influence of biomass burning plumes on HONO chemistry in eastern China. Atmos. Chem. Phys. 15, 1147–1159. https://doi.org/10.5194/acp-15-1147-2015.

Pavlovic, R., Chen, J., Anderson, K., Moran, M.D., Beaulieu, P.A., Davignon, D., Cousineau, S., 2016. The FireWork air quality forecast system with near-real-time biomass burning emissions: Recent developments and evaluation of performance for the 2015 North American wildfire season. J. Air Waste Manage. 66, 819–841. https://doi.org/10.1080/10962247.2016.1158214.

Pechony, O., Shindell, D.T., 2009. Fire parameterization on a global scale. J. Geophys. Res. Atmos. 114, D16115. https://doi.org/10.1029/2009JD011927.

Peterson, D., Hyer, E., Wang, J., 2013. A short-term predictor of satellite-observed fire activity in the North American boreal forest: Toward improving the prediction of smoke emissions. Atmos. Environ. 71, 304–310. https://doi.org/10.1016/j.atmosenv.2013.01.052.

Qu, C.S., Li, B., Wu, H.S., Giesy, J.P., 2012. Controlling Air Pollution from Straw Burning in China Calls for Efficient Recycling. Environ. Sci. Technol. 46, 7934–7936. https://doi.org/10.1021/es302666s.

Rumelhart, D.E., Hinton, G.E., Williams, R.J., 1986. Learning Representations by Back-Propagating Errors. Nature 323, 533–536. https://doi.org/10.1016/B978-1-4832-1446-7.50035-2.

Stair, O., Berberoglu, S., Donmez, C., 2016. Mapping regional forest fire probability using artificial neural network model in a Mediterranean forest ecosystem. Geomatics, Nat. Hazards Risk 7, 1645–1658. https://doi.org/10.1080/19475705.2015.1084541.

Shrivastava, M., Fast, J., Easter, R., Gustafson, W.I., Zaveri, R.A., Jimenez, J.L., Saide, P., Hodzic, A., 2011. Modeling organic aerosols in a megacity: comparison of simple and complex representations of the volatility basis set approach. Atmos. Chem. Phys. 11, 6639–6662. https://doi.org/10.5194/acp-11-6639-2011.

van der Werf, G.R., Randerson, J.T., Giglio, L., Collatz, G.J., Kasibhatla, P.S., Arellano, A.F., 2006. Interannual variability in global biomass burning emissions from 1997 to 2004. Atmos. Chem. Phys. 6, 3423–3441. https://doi.org/10.5194/acp-6-3423-2006.

van der Werf, G.R., Randerson, J.T., Giglio, L., Collatz, G.J., Mu, M., Kasibhatla, P.S., Morton, D.C., DeFries, R.S., Jin, Y., van Leeuwen, T.T., 2010. Global fire emissions and the contribution of deforestation, savanna, forest, agricultural, and peat fires (1997-2009). Atmos. Chem. Phys. 10, 11707–11735. https://doi.org/10.5194/acp-10-11707-2010.

van der Werf, G.R., Randerson, J.T., Giglio, L., van Leeuwen, T.T., Chen, Y., Rogers, B.M., Mu, M., van Marle, M.J.E., Morton, D.C., Collatz, G.J., Yokelson, R.J., Kasibhatla, P.S., 2017. Global fire emissions estimates during 1997–2016. Earth Syst. Sci. Data 9, 697–720. https://doi.org/10.5194/essd-9-697-2017.

Vasconcelos, M.J.P., Silva, S., Tome, M., Alvim, M., Pereira, J.M.C., 2001. Spatial prediction of fire ignition probabilities: Comparing logistic regression and neural

networks. Photogramm. Eng. Rem. Sens. 67, 73–81.
Vasilakos, C., Kalabokidis, K., Hatzopoulos, J., Matsinos, I., 2009. Identifying wildland fire ignition factors through sensitivity analysis of a neural network. Nat. Hazards 50, 125–143. https://doi.org/10.1007/s11069-008-9326-3.
Wang, L.L., Xin, J.Y., Li, X.R., Wang, Y.S., 2015. The variability of biomass burning and its influence on regional aerosol properties during the wheat harvest season in North China. Atmos. Res. 157, 153–163. https://doi.org/10.1016/j.atmosres.2015.01.009.
Wang, Q., Ma, S.-q., Guo, J.-p., Zhang, T.-l., Yu, H., Xu, L.-p., 2009. Effects of air temperature on maize growth and its yield. Chin. J. Ecol. 28, 255–260. https://doi.org/10.13292/j.1000-4890.2009.0020.
Wang, T.J., Jiang, F., Deng, J.J., Shen, Y., Fu, Q.Y., Wang, Q., Fu, Y., Xu, J.H., Zhang, D.N., 2012. Urban air quality and regional haze weather forecast for Yangtze River Delta region. Atmos. Environ. 58, 70–83. https://doi.org/10.1016/j.atmosenv.2012.01.014.
Wiedinmyer, C., Akagi, S.K., Yokelson, R.J., Emmons, L.K., Al-Saadi, J.A., Orlando, J.J., Soja, A.J., 2011. The Fire INventory from NCAR (FINN): a high resolution global model to estimate the emissions from open burning. Geosci. Model Dev. (GMD) 4, 625–641. https://doi.org/10.5194/gmd-4-625-2011.
Wu, Y.H., Han, Y., Voulgarakis, A., Wang, T.J., Li, M.M., Wang, Y., Xie, M., Zhuang, B.L., Li, S., 2017. An agricultural biomass burning episode in eastern China: Transport, optical properties, and impacts on regional air quality. J. Geophys. Res. Atmos. 122, 2304–2324. https://doi.org/10.1002/2016JD025319.
Xing, X.W., Zheng, W.Y., Peng, Q.P., Gu, X.W., 2014. Guangdong Statistical Yearbook of Agriculture 2014. China Statistics Press, Beijing.
Yan, X.Y., Ohara, T., Akimoto, H., 2006. Bottom-up estimate of biomass burning in mainland China. Atmos. Environ. 40, 5262–5273. https://doi.org/10.1016/j.atmosenv.2006.04.040.
Zaveri, R.A., Easter, R.C., Fast, J.D., Peters, L.K., 2008. Model for Simulating Aerosol Interactions and Chemistry (MOSAIC). J. Geophys. Res. Atmos. 113, D13204. https://doi.org/10.1029/2007JD008782.
Zha, S.P., Zhang, S.Q., Cheng, T.T., Chen, J.M., Huang, G.H., Li, X., Wang, Q.F., 2013. Agricultural Fires and Their Potential Impacts on Regional Air Quality over China. Aerosol Air Qual. Res. 13, 992–1001. https://doi.org/10.4209/aaqr.2012.10.0277.
Zhao, H.M., Zhang, X.L., Zhang, S.C., Chen, W.W., Tong, D.Q., Xiu, A.J., 2017. Effects of Agricultural Biomass Burning on Regional Haze in China: A Review. Atmosphere Basel 8, 88. https://doi.org/10.3390/atmos8050088.
Zhuang, Y., Li, R.Y., Yang, H., Chen, D.L., Chen, Z.Y., Gao, B.B., He, B., 2018. Understanding Temporal and Spatial Distribution of Crop Residue Burning in China from 2003 to 2017 Using MODIS Data. Rem. Sens. 10, 390. https://doi.org/10.3390/rs10030390.